

Cosolvent, Ions, and Temperature Effects on the Structural Properties of Cecropin A–Magainin 2 Hybrid Peptide in Solutions

Edita Sarukhanyan,^{1,2} Giuseppe Milano,^{2,3} Danilo Roccatano¹

¹ School of Engineering and Science, Jacobs University Bremen, Campus Ring 1, D-28759 Bremen, Germany

² Dipartimento di Chimica e Biologia and NANOMATES, Research Centre for NANOMaterials and nanoTEchnology at Università di Salerno, I-84084 via Ponte don Melillo Fisciano (SA), Italy

³ IMAST Scarl-Technological District in Polymer and Composite Engineering, P.le Fermi 1, 80055 Portici (NA), Italy

Received 16 January 2014; revised 8 July 2014; accepted 21 July 2014

Published online 24 July 2014 in Wiley Online Library (wileyonlinelibrary.com). DOI 10.1002/bip.22529

ABSTRACT:

Antimicrobial peptides are promising alternative to traditional antibiotics and antitumor drugs for the battle against new antibiotic resistant bacteria strains and cancer maladies. The study of their structural and dynamics properties at physiological conditions can help to understand their stability, delivery mechanisms, and activity in the human body. In this article, we have used molecular dynamics simulations to study the effects of solvent environment, temperature, ions concentration, and peptide concentration on the structural properties of the antimicrobial hybrid peptide Cecropin A–Magainin 2. In TFE/water mixtures, the structure of the peptide retained α -helix contents and an average hinge angle in close agreement with the experimental NMR and CD measurements reported in literature. Compared to the TFE/water mixture, the peptide simulated at the same ionic concentration lost most of its α -helix structure. The increase of peptide concentration at both 300 and 310 K resulted in the peptide aggregation. The peptides in the complex retained the initial N-ter α -helix segment during all the simulation. The α -helix stabilization is further enhanced

in the high salt concentration simulations. The peptide aggregation was not observed in TFE/water mixture simulations and, the peptide aggregate, obtained from the water simulation, simulated in the same conditions did dissolve within few tens of nanoseconds. The results of this study provide insights at molecular level on the structural and dynamics properties of the CA-MA peptide at physiological and membrane mimic conditions that can help to better understand its delivery and interaction with biological interfaces. © 2014 Wiley Periodicals, Inc. *Biopolymers* 103: 1–14, 2015.

Keywords: molecular dynamics simulations; peptide aggregation; 2,2,2-trifluoroethanol; peptide conformation; antimicrobial peptide

This article was originally published online as an accepted preprint. The “Published Online” date corresponds to the preprint version. You can request a copy of the preprint by emailing the *Biopolymers* editorial office at biopolymers@wiley.com

INTRODUCTION

Antimicrobial peptides (AMP) are produced by many organisms, including mammals, amphibians, and insects.^{1–7} It has been recognized that these peptides play an important role in both the host defense system and the innate immunity. For this reason, they are considered as possible alternative to traditional antibiotics for the battle against new drug resistant bacteria strains and cancer cells.^{8,9} In the quest for peptides with improved antibacterial and anticancer activities (but

Additional Supporting Information may be found in the online version of this article.

Correspondence to: Danilo Roccatano; e-mail: d.roccatano@jacobs-university.de

Contract grant sponsor: University of Salerno and Jacobs University of Bremen for the financial support

© 2014 Wiley Periodicals, Inc.

without toxic effects on healthy eukaryotic cells), the use of systematic combination of natural peptide amino acids sequences resulted in different novel hybrid peptides.^{10–12} Among these, the ones recently obtained by the combination of the Cecropin A (CA) and the Magainin 2 (MA) peptides, have shown promising anticancer and antibacterial activity.^{10–12} CA is a 37 amino acids antimicrobial peptide present in the hemolymph of *Hyalophora cecropia* pupae,^{2,4,10,11,13–15} and MA is 23 amino acids long peptide extracted from the skin of the African clawed frog, *Xenopus laevis*.^{1,4,5,16,17} Both, CA and MA have strong lytic activities against Gram-positive and Gram-negative bacteria without toxic effects for eukaryotic cells, such as human erythrocytes.^{1,2,4,5} Among the different hybrid peptides derived from CA and MA peptides, the one composed by combining the residues 1–8 of first and 1–12 of second one with the resulting sequence KWKLFKKI-GIGKFLHSAKFF-CONH₂, showed better antibacterial and antitumor activity compared to the starting peptides.^{12,18,19} The structure of the CA-MA peptide in solution has been investigated by Nuclear Magnetic Resonance (NMR) spectroscopy and circular dichroism (CD).^{12,20,21} The structure has been determined for concentrations up to 100 µg/ml and in three different membrane mimic solutions environments: 50% (v/v) trifluoroethanol(TFE)/water solution,²¹ 30 mM sodium dodecylsulfate (SDS)²¹ and dodecylphosphocholine (DPC)¹⁸ micelle. The NMR peptide conformation in 50% TFE/water mixture have been described²¹ but, unfortunately, the coordinates are not available. From the CD measurements in phosphate buffer, the α -helix percentage was found as low as 5.9% was observed.²¹ On the contrary, in 50% TFE and 30 mM SDS, it increases up to 54.4% and 14.1%, respectively.²¹ The only available NMR conformations of the CA-MA peptide are those obtained in DPC micelles. For these conformations, the average content of α -helix structure, calculated using the DSSP program (see Results section), is $45 \pm 10\%$. The average conformation consists of two α -helices separated by a flexible hinge region with sequence G9-I10-G11.^{18,21} Experimental studies suggest that the α -helical propensity of AMP and the presence of a flexible hinge region play an important role in the mechanism of pore formation throughout cell membrane, and, therefore, in their bactericidal and tumoricidal capabilities.^{18,21} In particular for the CA-MA peptide, the deletion of G9-I10-G11 as well as the substitution of the I10 with proline resulted in a decrease of bactericidal activity against *Bacillus subtilis* and *Escherichia coli*, and anticancer activity against four different cancer cell lines. On the contrary, the substitution of the sequence with proline (CA-MA-P2 peptide) retained a similar antimicrobial activity and showed even better anticancer activities than CA-MA.^{18,21}

Another important aspect, not yet investigated at molecular level for this peptide, is its actual “disordered” conformation

in buffer solution and the effects of ionic strength, temperature, and peptide concentration on it. The last ones can influence the mechanism of interaction with the cell membrane, and, hence its antibiotic and antitumor activity. Concerning ionic strength of the buffer solution, experimental studies of the similar P18 peptide (the aforementioned CA-MA-P2 with in addition the Ser14Leu substitution) in the presence of physiological NaCl concentration (100–200 mM) have evidenced a strong resistance on antimicrobial activity against bacterial strains and the fungus *C. albicans* compared to the MA peptide.²² Recent computational studies have also suggested the importance of the peptide aggregation in driving mechanism of pore formations in lipid bilayers.^{23,24} The aggregation of the peptide in small soluble clusters in solution can provide an efficient recruiting mechanism to increase its local concentration on the cellular surface and promote the pore formation more efficiently.

Molecular dynamics (MD) simulation is a powerful method to study at atomistic level disordered structures of peptides and small proteins in solution being, nowadays, possible to easily reach simulation time scales of several 100 ns at which these phenomena become interesting. In this article, we have used this computational approach with the aim to study the behavior of the CA-MA hybrid peptide in aqueous media at different ionic strength conditions, temperatures, and peptide concentrations. We report results of MD simulations of the CA-MA peptide in pure water and in the presence of 150 mM NaCl (similar to the concentration in the human blood plasma²⁵), and at two different temperatures (300 and 310 K, 37°C, the average temperature of the human body) and peptide concentrations. In addition, simulations of two different peptide concentrations in the model of membrane mimic environment constituted by a mixture of 50% (v/v) TFE/water are also reported.

The paper is organized as follows. In the Material and Methods section, the technical details of the MD simulations are provided. Thereafter, the results obtained out of the simulations of single and four CA-MA peptides in different conditions are reported. In the Discussion and Conclusion section, the results will be compared and summarized with the available experimental data and MD simulations studies of similar peptides.

MATERIAL AND METHODS

System Setup and Force Field

As starting coordinates of CA-MA hybrid peptide, the first NMR model structure of the 20 lowest-energy structures calculated from the NMR data of the peptide in DPC micelle [Protein Data Bank (PDB), entry code 1D9J,¹⁸ see Figure S1A of Supporting Information] was

Table I Summary of the Composition and Temperature Condition of the Simulated Systems.

	Simulation Reference Code ^a	No of Peptides	No of Water Molecules	No of Na ⁺ Ions	No of Cl ⁻ Ions	No of TFE Molecules	Temp. (K)	Sim. Length (ns)
1	1W300	1	33,082	0	8	0	300	500
2	1I300	1	32,906	88	96	0	300	500
3	1I310	1	32,906	88	96	0	310	500
4	4W300	4	32,683	0	32	0	300	500
5	4I300	4	32,509	87	119	0	300	500
6	4I310	4	32,509	87	119	0	310	500
7	W300	0	33,155	8	8	0	300	10
8	1T300	1	16,121	0	8	4310	300	250
9	4T300S	4	15,868	0	32	4251	300	250
10	4T300L	4	15,868	0	32	4251	300	250

^aThe numbers on the left and right side of the letter indicate the number peptides in the simulation and the temperature, respectively. The capital letter stands for: W, water; I, high ion concentration; T, TFE/water mixture, respectively. Example: 1W300 is the simulation of single peptide in water at 300 K. The letter *S* and *L* in the last two simulations indicate the different initial peptides coordinates used in the two cases.

used. The peptide was centered in cubic boxes of size 10 nm and the empty space was filled with water molecules by stacking an equilibrated box of 216 water molecules. The water molecules within 0.25 nm from the solute atoms were removed. Cl⁻ counter ions were added to keep the system neutral for the simulation boxes with one and four CA-MAs. Two set of MD simulations at different ionic strength were performed. In the low salt concentration (LSC) simulations, only the Cl⁻ ions necessary to neutralize the positive charges on the peptide(s) were added. For the simulations at high salt concentration (HSC), beside the neutralizing counter ions, extra Na⁺ and Cl⁻ ions were added to obtain a final concentration of ~150 mM. In addition, simulations with four peptides (corresponding to a concentration of 6.45 mM) were performed to study the effect of temperature and ion concentration on the peptide aggregation. The first NMR model from the PDB was used as starting structure of the four peptides was used for the simulations 4W300, 4I300, and 4I310 (Fig. S1B of Supporting Information). For water, the simple point charge (SPC) model was used in all the simulations.²⁶ For the peptide and ions the GROMOS54a7²⁷ force field was used.

To study the effect of membrane mimic environment, simulations in 50% by volume of TFE-containing aqueous solutions were performed at the same peptide concentrations. Although the structure of the peptide in TFE/water has not yet been deposited in the PDB, we decided to study the peptide in this environment since a well-tested^{28,29} GROMOS model for MD simulations of TFE solvent is available³⁰ and several previous MD studies of different peptides in this solvent have been conducted by one of the author.^{28,29,31} This model has been accurately optimized to reproduce the properties of mixtures with water.³⁰ In particular, two simulations were carried out to study the effect of the TFE cosolvent on the peptide aggregation. In the first one (4T300S), the same NMR conformation was used as starting structure for all the four peptides (Fig. S1B of Supporting Information) present in the simulation box. In the second one (4T300L), the coordinates of the four peptides aggregate obtained after 500 ns of the 4W300 simulation (Fig. S1C of Supporting Information) were used as starting conformation.

In Table I, a summary of the composition and temperature conditions of the simulated systems is reported.

MD Simulations

MD simulations were performed using GROMACS (version 4.5.5) software package. The LINCS algorithm³² was applied in order to constraint the bond lengths during the simulation. The integration time step was set equal to 2 fs. The temperature and pressure were maintained to the reference values ($T = 300$ and 310 K, $P = 1$ bar) using the Berendsen thermostat and barostat³³ with the coupling time constant of $\tau_T = 0.1$ ps for temperature and $\tau_p = 0.5$ ps for pressure, respectively. The isothermal compressibility of 4.5×10^{-5} bar⁻¹ was used for all the simulation. Particle mesh Ewald (PME) method³⁴ was applied for the long-range interactions with a real space cutoff of 1 nm, a Fourier mesh spacing of 0.12 nm. The Lennard-Jones interactions were calculated using the cutoff of 1.4 nm. The protonation state of the peptide amino acids in all simulations was assumed the one at neutral pH. All the systems were initially energy minimized using steepest descent algorithm of at least 1000 steps in order to relax the system and remove too close contacts among atoms. Hence, they were gradually heated from 50 K up to the simulation temperature within 1 ns of simulation. The length of the final production run of each simulation is reported in Table I.

Analysis of the MD Trajectories

The VMD³⁵ program was used to render the images of the molecular structures. Gromos clustering method³⁶ of the peptide conformations has been used to analyze the structural changes during the simulation. A cutoff criterion of 0.25 nm on the backbone root mean square deviations (RMSD) among all the conformations in a trajectory is used to classify the structures in different clusters. A total of 10,000 structures, sampled every 50 ps from the 500 ns trajectories, have been used for the analysis. The conformation with the least deviation from the other structures in the same cluster is considered as the representative one (median structure) of the cluster. Secondary structure analysis was performed referring to Kabsch and Sander's algorithm.³⁷ The radial distribution functions (RDFs) for the specific ion were calculated with respect to C- α atom of each amino acid residue and represented all together as two-dimensional "heat" maps. In this representation the x - and y -axes represents the distance from C- α atoms, and the amino acids, respectively. The colors in the plots codify for the RDF

Table II Hinge Angles, Segment Lengths, and Their Form Factors of the Peptides Calculated in the Last 50 ns of all the Simulations

Peptide Set/Simulation	Hinge Angle (degrees)	Length of Segment 1 (nm)	Length of Segment 2 (nm)	Form Factor for Segment 1	Form Factor for Segment 2
IDEAL	174	0.8	0.9	2.6	2.9
NMR	143 ± 21	0.9 ± 0.1	0.90 ± 0.02	3.0	3.0
1T300	140 ± 20	1.0 ± 0.1	1.0 ± 0.2	3.3	2.9
4T300S	150 ± 10	1.0 ± 0.1	0.9 ± 0.1	3.2	2.8
	150 ± 10	0.97 ± 0.05	0.9 ± 0.1	3.3	2.9
	160 ± 10	0.8 ± 0.10	0.89 ± 0.05	2.6	2.7
	100 ± 60	1.0 ± 0.2	0.9 ± 0.1	3.3	2.8
4T300L	100 ± 40	1.3 ± 0.2	0.9 ± 0.1	5.1	2.3
	110 ± 30	1.4 ± 0.1	1.4 ± 0.2	6.0	5.0
	65 ± 46	1.4 ± 0.1	1.5 ± 0.2	5.0	5.1
	120 ± 30	1.4 ± 0.1	1.0 ± 0.1	5.5	2.9

distributions values. The number of TFE (n_{TFE}) and water ($n_{\text{H}_2\text{O}}$) molecules at 0.6 nm from the $C\alpha$ atoms of each amino acid in the peptide was used to estimate the relative fractional TFE concentration as:

$$\text{RFTC} = \frac{n_{\text{TFE}} / (n_{\text{TFE}} + n_{\text{H}_2\text{O}})}{N_{\text{TFE}} / (N_{\text{TFE}} + N_{\text{H}_2\text{O}})} \quad (1)$$

where N_{TFE} and $N_{\text{H}_2\text{O}}$ are the total number of TFE and water molecules in the simulation box (Table I). The RFTC gives a qualitative estimation of the local TFE concentration around the amino acids of the peptide with respect to the average one.

Calculation of the Peptide Hinge Angle

For the calculation of the hinge angle, we assume that the hinge occurs at the G9-I10-G11 amino acids as observed in the NMR structures. The $C\alpha$ atoms of the two segment 2–10 and 10–19 was used to calculate the angle. The hinge angle (θ) was calculated using matrix of the momentum of the coordinates. The methods consist in the calculation of the principal axis of the two sets of atoms by using the covariance matrix of the coordinates calculated as follows:

$$\mathbf{C} = \frac{1}{N} \begin{pmatrix} \sum x^2 & \sum xy & \sum xz \\ \sum yx & \sum y^2 & \sum yz \\ \sum zx & \sum zy & \sum z^2 \end{pmatrix} \quad (2)$$

where the summation is over the number N of the $C\alpha$ of the considered peptide segment. By diagonalizing the matrix \mathbf{C} , three eigenvectors, and the corresponding eigenvalues (λ) are obtained. The eigenvectors give the directions (cosine directors) of the principal axis along with the $C\alpha$ coordinates are distributed. In the case of α -helix the eigenvector with the largest eigenvalue (λ_1) is a good approximation to the helix axis. The hinge angle was calculated using the inner product of two vectors collinear to the largest eigenvectors from each peptide segments, with origin the $C\alpha$ of I10 and pointing towards the beginning and the end of the peptide, respectively. The length of the segments is calculated as $2\sqrt{\lambda_1}$. Finally, the form factor for the segment is given by:

$$f = \frac{(\lambda_2 + \lambda_3)}{2\lambda_1} \quad (3)$$

the length of each segment from the largest eigenvector and the corresponding form factor provide comparative factors for the shape of the peptide segments. In Table II, the values of the hinge angle and the other structural parameters for an ideal extended α -helix (IDEAL) generated using the program VMD are reported.³⁵ It can be noticed that the hinge angle is not exactly 180 but still a close approximation.

RESULTS

Structure of the Single Peptide in the TFE/Water Mixture

In Figure 1, the secondary structure changes versus time for the single peptide in 50% TFE/water solution is reported. The initial α -helix content slowly decreases in the first 125 ns and reaches a stable value for the rest of the simulation. The average percentage of secondary structure, calculated for the last 150 ns, is equal to $\sim 44.5\%$ (see the right side of Figure 1, violet bar). This value is consistent with the secondary structure content calculated using the DSSP program from the 20 deposited NMR conformations of the peptide in the DPC micelle is equal to $45 \pm 10\%$. This result is in good quantitative agreement with experimental CD measurements providing percentages of helicity ranging from 35.1% at $\text{pH} = 4.0$ ²⁰ to 54.4% at $\text{pH} = 7.0$.²¹

The RFTC per amino acid (Figure S11 of Supporting Information), calculated in the last 25 ns of the simulation, gives an average value of 2.2 ± 0.5 with the maximum value in correspondence of the middle of the peptide (IGIG region), where the TFE concentration is three times higher than the bulk. The increase of TFE concentration around peptides (coating effect) was also observed in the AMP Melittin and other secondary structure forming peptides.³¹

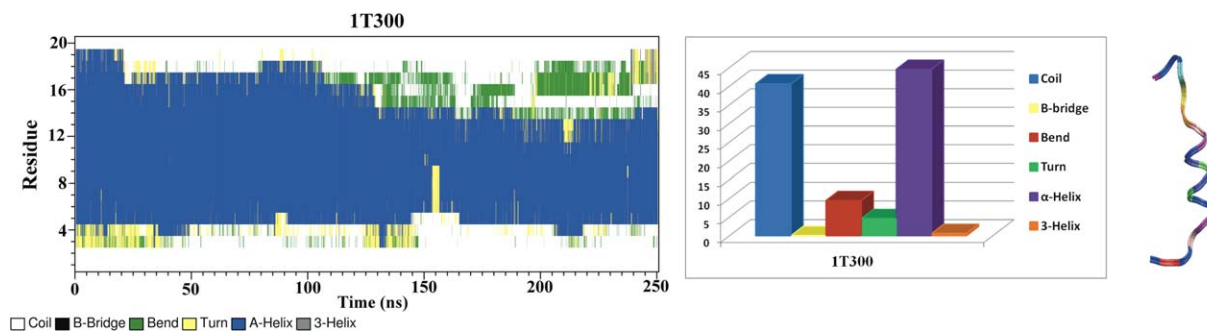


FIGURE 1 Secondary structures changes during the time for single peptide simulation in 50% (v/v) TFE-containing aqueous solution. At the right side from the plot is shown the percentage of average secondary structure for the corresponding simulation within the last 100 ns and the peptide conformation at 250 ns (the last configuration).

Finally, an average value of 140 ± 20 for the hinge angle was obtained from the last 50 ns of simulation (Table II). This value is in close agreement with the experimental value of 143 ± 21 obtained from the experimental structures of the peptide in DPC micelle (Table II).

Structure of the Single Peptide in Water Solution

Figure 2 shows the changes during the simulation time of the CA-MA peptide secondary structures in LSC and HSC conditions, and at both $T = 300$ K and 310 K. The percentage of secondary structure for the last 250 ns has been calculated and the average values are presented as histogram plots on the right side of the figure. For the simulation 1W300 (Figure 2, top), a sharp decrease of α -helix structure for the first 15 amino acids occurs in the first 20 ns followed by the formation of a β -hairpin in the C-terminal region of the peptide. The increase of the salt concentration, in the HSC simulations, reduces the kinetics of α -helix unfolding (Figure 2, second plot), with the results that the average helical content is 2.5 times higher than in the low salt concentration simulations. Finally, the increase of the temperature till 310 K resulted in an irreversible loss of α -helix also in the region 15–20 (Figure 2, third plot). In this case, the peptide shows a similar contents of β -strands as in the 300 K simulation, but very low contents of α -helix (see right side of Figure 2). The low amount of α -helix is in qualitative agreement with experimental CD measurements on the conformations of the peptide in solution.^{12,18,21} In particular, the presence of 5.8% of α -helix structure for the 1I300 simulation (Figure 2, first chart, violet column bar) is consistent with the value of 5.9% reported from CD measurements of the CA-MA peptide in 10 mM sodium phosphate buffer (pH 7.2) at 25°C.²¹ Our model suggests that at 300 K the peptide retains more α -helical structure at HSC than at LSC. However, at HSC and 310 K (physiological conditions) the α -helix disappears almost completely.

Cluster analysis has been performed for all single peptide simulations. In Figure S2 of Supporting Information, the cumulative number of clusters is reported. In all the simulations the number of cluster converges to plateau, but at different simulation times. For the simulation 1I300 (red curve), the curve plateaus to 69 clusters after 150 ns. At higher temperature (green curve) a larger variety of conformations are generated and the curve start to plateau to 150 clusters after 250 ns. For the low temperature LSC simulation (black curve) the convergence is slower with a temporary plateau at 69 clusters and a subsequent increase up to the final plateau of ~ 125 clusters after 400 ns. In Figure 3, all representative structures (RS) of the first five clusters are reported. For the system 1W300, the most abundant cluster contains 28% of total conformations with the median RS at time of 153 ns (Figure 3, first column). The RS has residues at positions L4, F5 and G9, I10 that form two β -strands with the turn region at positions K6, K7, and I8. A β -bridge is also observed at both N and C-terminals, including residues W2 and K19. The rest of peptide residues adopt turn or bend secondary structures. The second cluster contains 13.7% of the total conformations with the RS at 409 ns. The main secondary structure in this cluster mainly consists of two β -sheets, separated by turn. Finally, clusters 3, 4, and 5 contain together about 15% of total conformations. N-terminal region of the median structure of cluster three shows random coil conformation, while the last four residues in the C-terminal region form a α -helix. Median RS's of clusters 4 and 5 present β -sheet secondary structures in the N-terminal regions and by β -turns in the middle. C-terminal region is composed of the residues forming a α -helix for the cluster 4 and β -bridge for the cluster 5, respectively.

In the simulation 1I300, the first cluster represents the 71% of total number of the analyzed conformers (Figure 3, second column). The representative structure consists of a β -hairpin with two β -strands at positions K3, L4, and K12, F13 and α -helix at

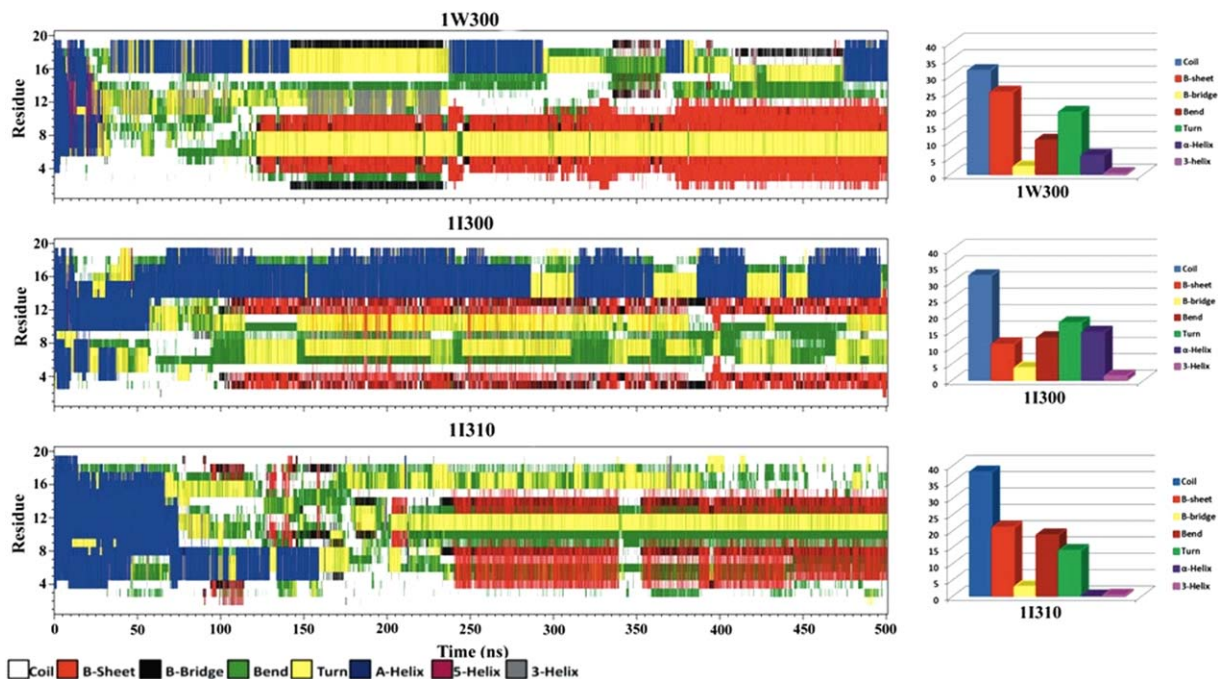


FIGURE 2 Secondary structures changes during the time for single peptide simulation in water at $T = 300$ K (first plot), 150 mM NaCl solution at $T = 300$ K (second plot) and at $T = 310$ K (third plot). At the right side from the plots are shown percentages of average secondary structure for the corresponding simulations.

the C-terminal residues 15–19 (HSAKK). The clusters 2–5 contain in total only $\sim 12\%$ of the total conformers population and are comparably populated ($\sim 3\%$). The representative clusters show an abundance of β -strands structures with the exception of clusters 2 and 5 in which a segment of α -helix is present at positions 13–19 (FLHSAKK) and 10–14 (IGKFL), respectively.

In the third column of Figure 3, the RSs of the clusters for the system 1I310 are reported. The percentage of population for the different clusters resembles the one from the 1W300 simulation. In addition, they show similar secondary structure composition. In particular, the presence of β -sheet formed by the residues at positions 4–8 (LFKKI) and 13, 14 (FL) with bend and turn regions in between. Amino acid residues localized near to the C-terminal for the RS of cluster 1 have bend and turn secondary structures, whereas for the RS of cluster 2, amino acid residues adopt mostly random coil conformation. For cluster 3 the RS is random coiled with the exception of residues at positions 5–8 (FKKI) that form a α -helix. The last two representative structures of clusters 4 and 5 are mainly in α -helical conformation.

Distribution of Ions Around the Peptide

In Figure 4 the graph representing the RDFs of the Cl^- ions for the systems 1I300 and 1I310 are presented. The positions of the peaks of the RDF for the Cl^- ions show a tendency to

bind the positively charged peptide. In particular, the Cl^- ions tend to localize in correspondence of the positively charged amino acids at positions 6, 7, 18, 19, at both 300 K and 310 K. In comparison, the RDFs for Na^+ and water oxygen atoms do not show high-localized peaks around the peptide (see Figure S3 of Supporting Information).

The bottom panel of the Figure 4 reports the Cl^-/Na^+ ratios (calculated for each amino acids using the number of ions within 1.5 nm) at low (blue curve) and high temperatures (red curve) compared the total box ratio (bulk ratio and black line). The ratios show that the average concentration of the Cl^- ions is 6.4 times larger than the bulk phase, which shows again the preferential binding of Cl^- in comparison to the Na^+ ions.

Peptide Aggregation

Structural Properties of the Peptides. The effect of concentration on the structural properties of CA-MA has been analyzed with simulations of systems containing four peptides at the same conditions as for the single peptide. In Figures 5A and S4 of Supporting Information, the secondary structure variations along the simulations 4W300, and the histogram of the average (last 250 ns) percentage of secondary structure are reported. Peptides 1 and 4 retain both 30–40% of α -helix structure during the simulation. The α -helix comprises the






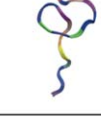









Cluster No.	1W300	1I300	1I310
1	 28 % 153 ns	 71 % 335 ns	 28.8 % 285 ns
2	 13.7 % 409 ns	 3.6 % 71 ns	 8.5 % 425 ns
3	 5.54 % 76 ns	 3.35 % 425 ns	 5.1 % 101 ns
4	 5.39 % 478 ns	 3 % 358 ns	 5.1 % 44 ns
5	 5 % 340 ns	 2.29 % 23 ns	 4.1 % 48 ns

FIGURE 3 First five representative structures obtained from cluster analysis out of the simulation of CA-MA hybrid peptide for the systems 1W300, 1I300, and 1I310. Color code for the amino acids in chain: K: blue, W: red, L: pink, F: magenta, I: green, G: violet, H: orange, S: yellow, A: cyan. Here N-terminal that starts with L is marked in blue, C: terminal, that has F is labeled in magenta.

amino acids 15–19 (HSAKK) for the peptide 1 and the 3–7 (KLFKK) and 9–18 (GIGKFLHSAKK) ones for the peptide 4. The peptide 2 loses completely the α -helical content after 430 ns and the peptide 3 after 85 ns. Peptide 3 forms a very stable β -hairpin after 100 ns of simulation involving the amino acids 2–7 (WKLFKK) and 11–17 (GKFLHSA) separated by the flexible hinge region 8–10 (IGI).

In Figure 6A, a diagram showing the minimum distances between peptides pairs, calculated considering only the backbone atoms, is reported. The low minimum distances, shown by red color band in the graph on the top, indicate the formation of two aggregation complexes that take place one, between peptide 1 and 4 (1:4), after 30 ns, and the other, between peptide 2 and 3 (2:3), after 430 ns, respectively. It is interesting to note that for the 1:4 complex the loss of α -helix structure is less in comparison to the 2:3 peptides complex. In Figure 6B,

the final structures of the peptides are reported. The residual α -helix fragments of the peptides 1 and 4 are antiparallel aligned while the third peptide bind with its residual α -helix on the top of the other two. The contacts occur on the hydrophobic side of each peptide mainly through aromatic residues. In particular, they take place between residues pairs F13-F13 and W2-W2 for the peptide 1 and peptide 4 (Figure 6B, top).

In the 4I300 simulation (Figure 6A, middle graph), an aggregate of three peptides is formed at the end of the simulation. Peptide 2 and 4 aggregate almost at the beginning of the simulation, and, after 90 ns, also the peptide three joins the complex. Also in this case, the interactions of the peptides in the complex (Figure 6B, middle) involve the aromatic residues F5-F20-F20 of the peptides 2, 3, and 4, respectively, and between the two W2 residues of the peptides 2 and 3. The aggregation prevents the unfolding of the initial α -helix

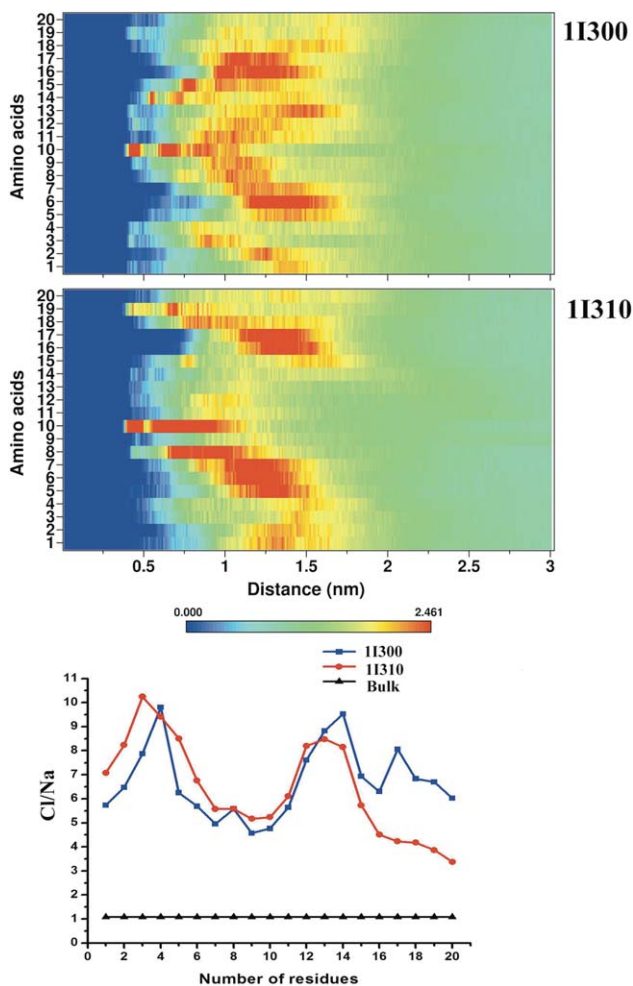


FIGURE 4 Top panels: Heat plots of the RDFs for the Cl^- , Na^+ , and O_w respect to each residue of CA-MA peptide in 150 mM NaCl solutions at $T = 300$ K (up) and $T = 310$ K (down). Bottom panel: Cl^-/Na^+ ratios for the systems 1I300 (blue), 1I310 (red), within 1.5 nm from C- α atoms of the peptide.

structure (Figure 5B, violet bars and Figure S5 (top panel) of Supporting Information), but more effectively than for the peptides at LSC (Figures 5A and S4 of Supporting Information). These results suggest that high salt and peptide concentration can cooperatively stabilize α -helix structure of the CA-MA peptide. To further verify the effect of the aggregation on the residual α -helix stability, the four peptides at the end of the 4I300 simulations each of them has been solvated in a box of water at the same ionic concentration as the 1I300 simulation. After equilibration (as described in the Method section), the systems have been run for 200 ns. In Figure S5 (bottom panel) of Supporting Information, the secondary structures of the 4 peptides during the simulation are reported. The peptides 2, 3, 4, forming the aggregate in the simulations 4I300, have lost the initial residual C-terminal α -helix and for peptide 2 and 4 β -strand structures start to form towards the end of the simula-

tions. Peptide 1 shows also a large destabilization of the residual α -helix structure with formation of β -bridge structures.

The increase of the temperature by 10 K results in a loss of α -helix structure and in the increase of β -strand structures (Figure S6 of Supporting Information and Figure 5C). In this case two aggregates are formed between peptide 1 and 4 after 150 ns, and by peptide 2 and 3 after 275 ns (Figure 6A, bottom graph). In the bottom panel of Figure S6 of Supporting Information, the configurations of the four peptides sampled every 20 ns starting at 50 ns for the peptide 1 and from 100 ns for the other peptides, are reported. In three peptides, the transition occurs through the progressive loss of the C-terminal helix and the formation of β -hairpin type structures. The time course of the backbone contacts within 0.6 nm is also reported in the diagram of Figure S7 of Supporting Information. An average number of ~ 22 contacts is observed between the peptide pairs involved in aggregation. In this case, the amino acids involved in interpeptide contacts are the residues H15–F13 of the peptide 1 and 4, and the two F13 of the peptides 2 and 3.

Structural Properties of Peptides in the TFE/Water Mixture.

The effect of the TFE cosolvent on the peptide aggregation has been investigated for both the systems 4T300S and 4T300L. The secondary structure changes for the four CA-MA peptides during the two simulations are shown in Figures S8 and S9 of Supporting Information. For the system 4T300S, there is a high tendency for all the peptides to retain their initial α -helical structure. In the case of the system 4T300L, only peptide 1 and 4 retain a residual α -helix. The β -hairpin structure in the peptide 3 unfolded after 150 ns. On the left side of Figure 7, histograms of the average percentage of secondary structure for the four peptides in the two simulations are reported. The average amount of α -helix for peptides 1, 2, and 3 from simulation 4T300S is over 60% with the exception of the peptide 4 that is only $\sim 30\%$ (Figure 7A). In the case of the 4T300L, only peptides 1 and 4 retained between 20 and 30% of the initial α -helix structure (Figure 7B).

In Table II, the average hinge angles for the four peptides from the 4T300S simulation are reported. For the first two, the angles are systematically larger than the isolated peptide in the same condition but still within the standard deviation of the NMR value (140 ± 10). The third one shows a larger hinge angle but a more compact shape of the segments (lower form factor) than the one from the single peptide simulation and the NMR structures. Finally, the last one has a significant smaller hinge angle than the other three and also a larger standard deviation that evidence large fluctuations of the two α -helical segments.

On the right side of the Figure 7, the conformations of four CA-MA peptides at 250 ns for the corresponding systems are reported. In Figure S10 of Supporting Information, the

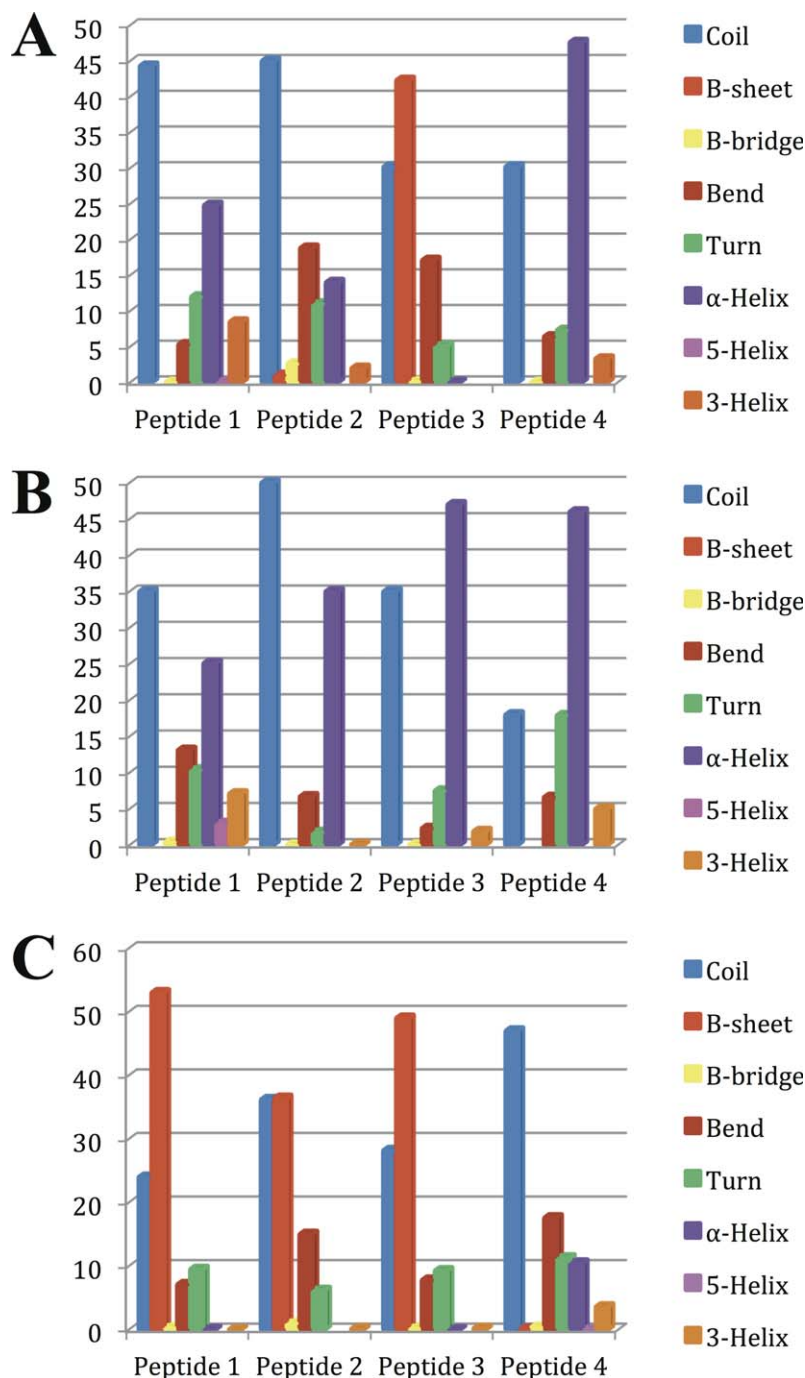


FIGURE 5 (A) Percentages of average secondary structure for the simulation of 4 CA-MA peptides in water at $T = 300$ K, in (B) 150 mM NaCl solution at $T = 300$ K, and at (C) $T = 310$ K for the last 250 ns.

number of contacts along the simulation is reported. For the simulation 4T300S, the peptides did not show binding contacts until the end of the simulation run.

Moreover, as shown in Figure 8 by the increase of the minimum distance, the peptides in the initial aggregated state (simulation 4T300L) disaggregate completely at the end of the 250

ns simulation. This is even more evident by looking in Figure S10 of Supporting Information to the P1-P4 and P2-P3 contacts, present at the beginning of simulation, that disappear completely within 90 ns.

The values of RFTC per amino acid (Figure S11 of Supporting Information), calculated in the last 25 ns of the simulations

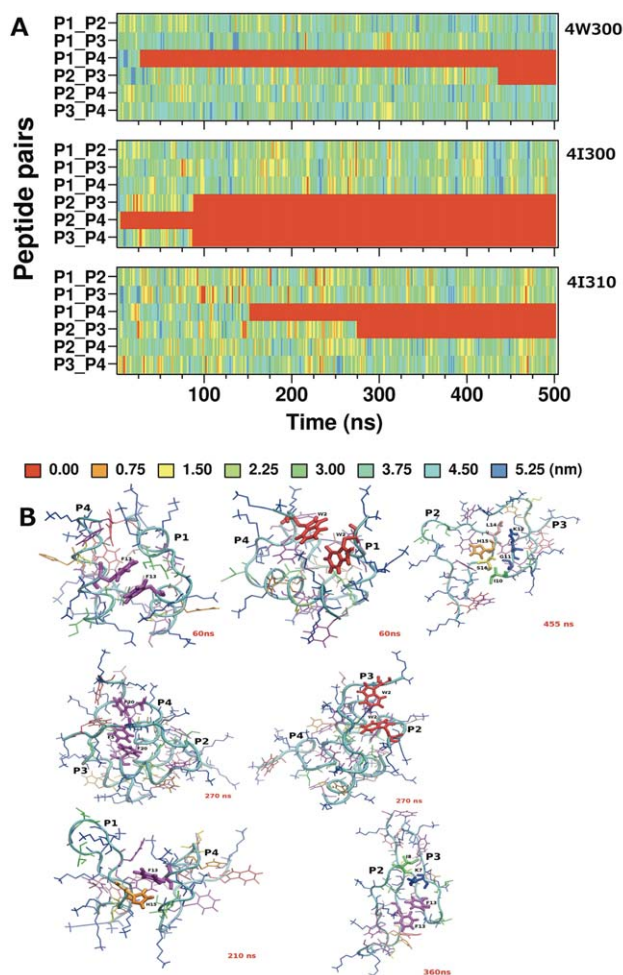


FIGURE 6 (A) Plots for the minimum distances versus time between the backbones of the peptides simulated in the system 4W300, 4I300, and 4I310. Colors are codifying the distances between the backbones of the peptide pairs. (B) Representation of the peptide's aggregated conformations from the simulations 4W300, 4I300, and 4I310, respectively. In licorice are highlighted amino acids, involved in contacts between the peptide pairs.

4T300S, give an average value of 2.4 ± 0.3 with a maximum of three in correspondence of the residue (IGIG) as observed in the simulations of the isolated peptide. In the case of the simulation 4T300L (Figure S12 of Supporting Information), an average RFTC value of 2.3 ± 0.3 and a maximum in correspondence of residues 4–16, in which the concentration is 2.5 times higher than the box concentration, is observed. The TFE coating effect can also provide a possible explanation of the peptide clusters disaggregation. In fact, the presence of TFE reduces the strength of the interactions between aromatic and apolar side chains of the peptides favoring their solution in a more hydrophobic solvent.³¹

In Figure S14 of Supporting Information, the cumulative numbers of cluster along the different high peptide concentra-

tion simulations are reported. In the system 4W300 (Figure S14 A of Supporting Information), the number of clusters for the peptides 1, 3, and 4 converges to different values (54, 85, and 25), and at different simulation times, 350 ns, 120 ns, and 25 ns, respectively. On the contrary, the number of clusters for the peptide 2 (red curve) grows constantly until the end of the simulation indicating a higher conformational flexibility than the other three peptides. In the case of simulation 4I300 (Figure S14 B of Supporting Information), the three peptides evidenced a rapid convergence to a number of clusters (in the interval 40–78) comparable to those observed in the 4W300 simulation. The peptide 4 (blue curve) shows the lowest conformational flexibility in all the simulations with a convergence after 150 ns to only 9 clusters. Finally, for the system 4I310 (Figure S14 C of Supporting Information) only peptide 1 (black curve) rapidly plateau to 58 clusters, the lowest number of clusters, while the other three reach after ~ 200 ns a relatively stable plateau to a larger value. The number of clusters obtained from the high peptide concentration simulations is rather similar to the one from the isolated peptide simulations (Figure S2 Supporting Information).

In Figure 9 the RS's of the most populated clusters of each peptide for the different simulations are shown. For each structure, the time of occurrence during the simulation and the cumulative percentage of cluster population are also reported. In the 4W300 simulation, the peptides are mostly uncoiled, except the peptide 4, which shows the presence of α -helix content. The initial helical content is better preserved in the most of the most abundant clusters from the 4I300 simulation. Finally, the first three RS's from the 4I310 simulation show mostly β -hairpin-like conformations and the fourth a small α -helix.

Distribution of Ions Around the Peptides. In Figure S15 of Supporting Information, the heat plots of RDFs for both ions with respect each residue of the 4 peptides in the 4I300 simulation are reported. The Cl^- ions tend to accumulate around the peptides 2, 3, and 4 depleting ions from the isolated peptide 1. This effect is quantitatively shown by the higher Cl^-/Na^+ ratios (Figure S15 of Supporting Information, bottom panel) for the peptides 2, 3, and 4 as compared to the peptide 1. The graphs also show that for the peptide 1 the highest values correspond to the amino acids G11 and A17, for the peptide 2 to the K7 and F13, for the peptide 3 to the F5, G9, and I10, and, finally, for the peptide 4 to the residues L14, A17, and K18, respectively.

In Figure S16 of Supporting Information, the heat plots of the RDFs for the Cl^- ions with respect to the residues of each peptide for the 4I310 simulation are reported. The binding of the ions to peptides 1, 2, and 3 is preferentially localized to the

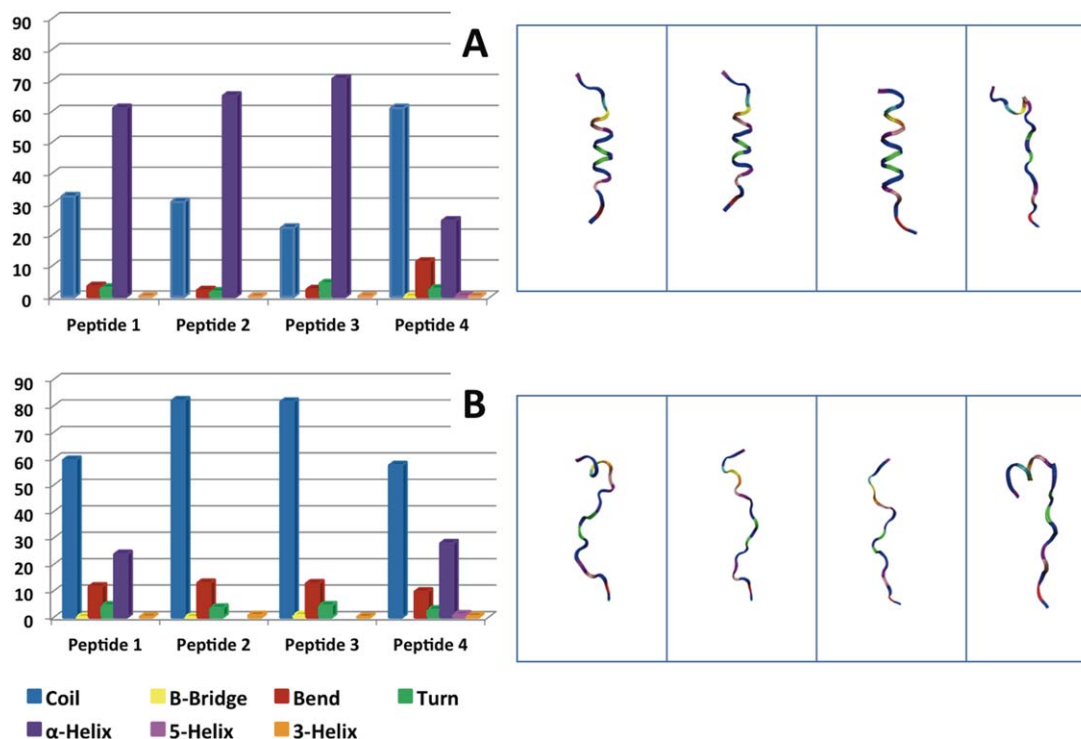


FIGURE 7 On the left side are shown the percentages of average secondary structure for the simulation of 4 CA-MA peptides in 50% (v/v) TFE-containing aqueous solutions for the systems (A) 4T300S and (B) 4T300L. On the right side are shown the corresponding conformations of four peptides at 250 ns.

central residues while for the peptide 4 to the terminal residues. The Cl^-/Na^+ ratios for the peptide 1, 2, and 3 (Figure S16 bottom panel) show a minimum at the residues 8–11, corresponding to the IGIG sequence, with the lowest value at positions G9 and I10. On the contrary, the peptide 4 has more constant values of the Cl^-/Na^+ ratio with a maximum for the G9 residue.

DISCUSSION AND CONCLUSIONS

In this article, we have performed MD simulations of one and four chains of the CA-MA hybrid peptides in 50% TFE/water mixture, and in water at different ionic strengths and temperatures. The 50% TFE/water mixture simulations, starting with the NMR conformation of one and four CA-MA peptides, have produced peptide conformations with α -helix content comparable to the experimental one. The role of nonaqueous solvent environment in the stabilization of secondary structure of peptides or in their aggregation is not yet a completely understood phenomenon at molecular level.³¹ In the case TFE/water mixtures, there are evidences from experimental measurements³⁸ and computational studies³¹ that the stabilization effect can occur via the preferential binding (coating) of the

peptide surface by the TFE molecules that both prevents water molecules to destabilize the backbone hydrogen bonding network and promotes a favorable hydrophobic environment for aromatic and apolar side chains.³⁹ Previous simulations studies using the same TFE model and force field type as in this work have shown that the α -helix structure of different AMP is retained consistently with experimental NMR data in the presence of fluorinated solvents as TFE^{28,40} and 1,1,1,6,6,6-

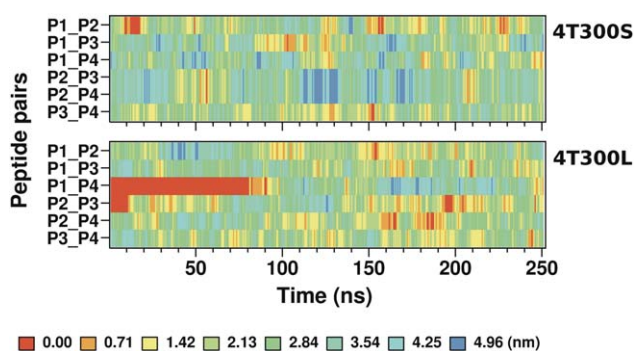


FIGURE 8 Plots for the minimum distance versus time between the backbones of the peptide pairs simulated in 50% (v/v) TFE-containing aqueous solutions for the systems 4T300S and 4T300L.













Cluster No.	4W300	4I300	4I310
1	 32 % 464 ns	 26 % 55 ns	 64 % 306 ns
2	 10.5 % 135 ns	 42 % 357 ns	 38 % 491 ns
3	 51 % 309 ns	 48 % 407 ns	 36 % 332 ns
4	 54 % 165 ns	 92 % 363 ns	 18 % 358 ns

FIGURE 9 Representative structures obtained from the cluster analysis out of the simulation of 4 CA-MA hybrid peptides in water at $T = 300$ K, in 150 mM NaCl at $T = 300$ K and at $T = 310$ K. The color code is the same as in the case of simulation of single peptide (see Figure 3).

hexafluoroisopropanol.²⁹ The stabilization of the α -helix regions in the CA-MA peptide simulation is determined by the same mechanisms as it is shown by the increase of the RFTC around the peptide at both low and high peptide concentrations. In addition, the results of the simulation starting from the peptide aggregate have shown that the TFE/water mixture solubilizes the peptide chains by improving the interactions with the solvent of the aromatic residues involved in intrachain interactions. The amount of α -helix observed in our simulations is also in good agreement with the experimental data.

The presence of a hinge in the α -helical structure associated with a G(X)_nG motif has been observed and studied in many AMP.^{41–44} The general opinion is that the hinge assists the peptide to deeply insert in the lipid bilayer from the N-terminal regions that contains invariably a tryptophan amino acid and determines the orientation of the insertion. Indeed, for the CA-MA peptide, the deletion of the flexible GIG region or the substitution of with GPG sequence compromises both its antimicrobial and tumoricidal activity but the substitution with

the only the proline amino acid in the CA-MA-P2 retains its antibiotic activity.^{18,21} This results suggested that the flexibility in this region central helix-hinge-helix is important for the antibiotic property of the peptide. The analysis of the average hinge angle in TFE showed that the peptide segment 1–10 and 10–20 form an angle similar to the one observed for the NMR conformation in DPC. The presence of a kinked peptide is recurrent in pore-forming peptides and the presence of previous studies have suggested that the hinge region is important for effective orientation of the peptide of the two helices within the bacterial cell membrane. Our simulations evidence the presence of hinged conformations in the presence of hydrophobic membrane mimic environment for both the peptide at low and high concentration (in the last case the angle is slightly larger and less fluctuating). Finally, the value of the hinge angle is comparable with the observed in the NMR structures in DPC and larger of the value (128 ± 30) observed for the modified peptide with the IGI sequence replaced with Pro amino acid.²¹

Depending on the type of ionic components, solution of salts can have stabilizing or destabilizing effects on peptides or proteins (Hofmeister effect).⁴⁵ There are several recent theoretical studies based on MD simulations, which are directed to understand salt effects on both structure and dynamics of polypeptides.^{46–49} In a recent simulation study, ion binding specificity to residue of the S6 ribosomal protein surface has been investigated.⁴⁸ Similarly to our results regarding to distribution of ions with respect to CA-MA peptide, they have found that at physiological concentrations (120 mM), Cl^- ions tends to have higher concentration on the protein surface compared to Na^+ . Also Dzubiella⁴⁹ have recently studied using MD simulations the effect of high concentration (2.5–2.7 M) of NaCl, KCl, NaI, and KI on the α -helicity of alanine-based peptides. The results of this study suggest that all these salts, with the exception of the NaI, play a stabilizing role on the secondary structure of the peptide.⁴⁹ In particular, a systematic increase of α -helicity has been observed for all the peptides simulated in the presence of salty environment. In our case, we have also found an increase of α -helicity for the peptides in 150 mM NaCl, despite the concentration of the salt is 18 times lower, than the one used by Dzubiella (2.7 M NaCl).

In all the simulations, the dominant secondary structure was the β -strand. The formation of β -strand structure was also observed in other MD simulations study of different AMP (but not all) in water.^{29,40} Unfortunately, from the available experimental data is not possible quantify if this results is consistent with the actual population of peptides with β -strand secondary structure contents present in solution. If it is not a conformation preference caused by the force field model then our simulations suggest that the peptide tend to adopt β -stranded structures at low concentration in aqueous solutions.

Simulations at the higher temperature of 310 K determine the complete disappearance of the N-terminal α -helix conserved at lower temperature simulations and the formation of β -stands.

At high peptide concentration, there is a rapid aggregation of the peptide chains that, in turn, promote a further stabilization of the secondary structure. The observed aggregate contains up to three peptides in an arrangement that resembles the tetrameric complex observed in the crystallographic structure of the Melittin peptide.⁵⁰ The contacts occur on the hydrophobic side of each peptide mainly through aromatic residues. A possible explanation of this effect is that the peptide aggregation reduces the water accessibility to the backbone delaying for this peptide the unfolding kinetics. One of the mechanism of pore formation in biological membranes by AMP involve the formation of peptide aggregates on the surface of the membrane.^{23,24} How these peptides are recruited at high concentration is still an unsolved problem. Our results

suggests the possibility of the formation of stable aggregates with a sufficient number of peptides that once on the surface of the biological membrane can induce the formation of the pore.

In conclusion, in this study, the effects of different solution conditions (salt concentration, temperature, solute concentration, and solvent) on the structural stability and association of the antimicrobial CA-MA peptide have been analyzed. Our simulations shown that the dilute peptide has low α -helix contents in water solution with tendency for β -stranded conformations. At higher peptide concentration the N-terminal α -helix can be stabilized by aggregation and ionic conditions. However, the aggregate are metastable and relatively small temperature changes can results in an increase of its β -strand contents. Soluble peptide aggregates may help to recruit peptides on the surface patches of bacterial and cancer cell at a concentration sufficiently high to provide an effective pore formation activity. Future simulation study on the interaction of single and aggregated peptide chains on the surface of lipid bilayer may help to clarify this hypothesis. The understanding of the details of this process can be useful for a better design of AMP for novel antibiotic or anticancer drug.

ACKNOWLEDGEMENT

This work was performed using the computer facilities of the Computational Laboratory for Analysis, Modeling, and Visualization (CLAMV) at Jacobs University Bremen.

REFERENCES

1. Bevens, C. L.; Zasloff, M. *Annu Rev Biochem* 1990, 59, 395–414.
2. Boman, H. G. *Cell* 1991, 65, 205–207.
3. Zasloff, M. *Curr Opin Immunol* 1992, 4, 3–7.
4. Boman, H. G. *Annual Review of Immunology* 1995, 61–92.
5. Maloy, W. L.; Kari, U. P. *Biopolymers* 1995, 37, 105–122.
6. Hancock, R. E. W.; Rozek, A. *FEMS Microbiol Lett* 2002, 206, 143–149.
7. Brogden, K. A. *Nat Rev Microbiol* 2005, 3, 238–250.
8. Sang, Y.; Blecha, F. *Anim Health Res Rev* 2008, 9, 227–235.
9. Hancock, R. E. W. *Lancet* 1997, 349, 418–422.
10. Steiner, H.; Hultmark, D.; Engstrom, A.; Bennich, H.; Boman, H. G. *Nature* 1981, 292, 246.
11. Lee, J. Y.; Boman, A.; Sun, C. X.; Andersson, M.; Jornvall, H.; Mutt, V.; Boman, H. G. *Proc Natl Acad Sci U S A* 1989, 86, 9159–9162.
12. Shin, S. Y.; Kang, J. H.; Lee, M. K.; Kim, S. Y.; Kim, Y. M.; Hahm, K. S. *Biochem Mol Biol Int* 1998, 44, 1119–1126.
13. Hultmark, D.; Steiner, H.; Rasmuson, T.; Boman, H. G. *Eur J Biochem* 1980, 106, 7–16.
14. Boman, H. G.; Faye, I.; Vonhofsten, P.; Kockum, K.; Lee, J. Y.; Xanthopoulos, K. G.; Bennich, H.; Engstrom, A.; Merrifield, R. B.; Andreu, D. *Dev Comp Immunol* 1985, 9, 551–558.
15. Lehrer, R. I.; Ganz, T. *Curr Opin Immunol* 1999, 11, 23–27.

16. Zasloff, M. *Proc Natl Acad Sci U S A* 1987, 84, 5449–5453.
17. Soravia, E.; Martini, G.; Zasloff, M. *FEBS Lett* 1988, 228, 337–340.
18. Oh, D.; Shin, S. Y.; Lee, S.; Kang, J. H.; Kim, S. D.; Ryu, P. D.; Hahm, K.-S.; Kim, Y. *Biochemistry* 2000, 39, 11855–11864.
19. Bechinger, B. *Biochim Biophys Acta* 1999, 1462, 157–183.
20. Oh, D.; Kim, Y.; Shin, S. Y.; Kang, J. H.; Hahm, K. S.; Kim, K. L. *J Pept Res* 1999, 53, 578–589.
21. Shin, S. Y.; Kang, J. H.; Jang, S. Y.; Kim, Y.; Kim, K. L.; Hahm, K.-S. *Biochim Biophys Acta* 2000, 1463, 209–218.
22. Shin, S. Y.; Yang, S. T.; Park, E. J.; Eom, S. H.; Song, W. K.; Kim, Y.; Hahm, K. S.; Kim, J. I. *Biochem Biophys Res Commun* 2002, 290, 558–562.
23. Sengupta, D.; Leontiadou, H.; Mark, A. E.; Marrink, S.-J. *Biochim Biophys Acta* 2008, 1778, 2308–2317.
24. Leontiadou, H.; Mark, A. E.; Marrink, S. J. *J Am Chem Soc* 2006, 128, 12156–12161.
25. Krebs, H. *Annu Rev Biochem* 1950, 19, 409–430.
26. Berendsen, H. J. C.; Postma, J. P. M.; van Gunsteren, W. F.; Hermans, J. In *Intermolecular Forces*. Pullman, B., Ed.; Springer: Netherland, 1981, pp 331–342.
27. Schmid, N.; Eichenberger, A. P.; Choutko, A.; Riniker, S.; Winger, M.; Mark, A. E.; vanGunsteren, W. F. *Eur Biophys J* 2011, 40, 843–856.
28. Roccatano, D.; Colombo, G.; Fioroni, M.; Mark, A. E. *Proc Natl Acad Sci* 2002, 99, 12179–12184.
29. Roccatano, D.; Fioroni, M.; Zacharias, M.; Colombo, G. *Protein Sci* 2005, 14, 2582–2589.
30. Fioroni, M.; Burger, K.; Mark, A. E.; Roccatano, D. *J Phys Chem B* 2000, 104, 12347–12354.
31. Roccatano, D. In *Advances in Protein and Peptide Sciences*; Dunn, B. M., Ed.; Bentham Science Publishers, 2013, pp 318–381.
32. Hess, B.; Bekker, H.; Berendsen, H. J. C.; Fraaije, J. G. E. M. *J Comput Chem* 1997, 18, 1463–1472.
33. Berendsen, H. J. C.; Postma, J. P. M.; Vangunsteren, W. F.; Dinola, A.; Haak, J. R. *J Chem Phys* 1984, 81, 3684–3690.
34. Darden, T.; York, D.; Pedersen, L. *J Chem Phys* 1993, 98, 10089–10092.
35. Humphrey, W.; Dalke, A.; Schulten, K. *J Mol Graph* 1996, 14, 33–38.
36. Daura, X.; Gademann, K.; Jaun, B.; Seebach, D.; van Gunsteren, W. F.; Mark, A. E. *Angew Chem Int Ed* 1999, 38, 236–240.
37. Kabsch, W.; Sander, C. *Biopolymers* 1983, 22, 2577–2637.
38. Gerig, J. T. *Annu Rep Nmr Spectro* 2008, 64, 21–76.
39. Jasanoff, A.; Fersht, A. *Biochemistry* 1994, 33, 2129–2135.
40. Chen, R.; Mark, A. E. *Eur Biophys J Biophys* 2011, 40, 545–553.
41. Haney, E. F.; Hunter, H. N.; Matsuzaki, K.; Vogel, H. J. *Biochim Biophys Acta* 2009, 1788, 1639–1655.
42. Perrin, B. S.; Tian, Y.; Fu, R. Q.; Grant, C. V.; Chekmenev, E. Y.; Wieczorek, W. E.; Dao, A. E.; Hayden, R. M.; Burzynski, C. M.; Venable, R. M.; Sharma, M.; Opella, S. J.; Pastor, R. W.; Cotten, M. L. *J Am Chem Soc* 2014, 136, 3491–3504.
43. Toke, O.; Banoczi, Z.; Kiraly, P.; Heinzmann, R.; Burck, J.; Ulrich, A. S.; Hudecz, F. *Eur Biophys J Biophys* 2011, 40, 447–462.
44. Wang, G. S. *J Biol Chem* 2008, 283, 32637–32643.
45. Lo Nostro, P.; Ninham, B. W. *Chem Rev* 2012, 112, 2286–2322.
46. Hess, B.; van derVegt, N. F. *Proc Natl Acad Sci* 2009, 106, 13296–13300.
47. Xie, W. J.; Gao, Y. Q. *Faraday Discuss* 2013, 160, 191–206.
48. Friedman, R. *J Phys Chem B* 2011, 115, 9213–9223.
49. Dzubiella, J. *J Phys Chem B* 2009, 113, 16689–16694.
50. Terwilliger, T. C.; Eisenberg, D. *J Biol Chem* 1982, 257, 6016–6022.

Reviewing Editor: David E. Wemmer